Applied Physics Letters ARTICLE scitation.org/journal/apl

Spin–orbit coupling proximity effect in MoS_2/Fe_3GeTe_2 heterostructures

Cite as: Appl. Phys. Lett. **120**, 043102 (2022); doi: 10.1063/5.0080505
Submitted: 1 December 2021 · Accepted: 10 January 2022 ·
Published Online: 24 January 2022

Zhiyin Tu,[1] Tong Zhou,[2] Thomas Ersevim,[3] Hasitha Suriya Arachchige,[4] Aubrey T. Hanbicki,[5] Adam L. Friedman,[5] David Mandrus,[4] Min Ouyang,[3] Igor Žutić,[2] and Cheng Gong[1,a)]

AFFILIATIONS

[1]Department of Electrical and Computer Engineering and Quantum Technology Center, University of Maryland, College Park, Maryland 20742, USA
[2]Department of Physics, University at Buffalo, State University of New York, Buffalo, New York 14260, USA
[3]Department of Physics, University of Maryland, College Park, Maryland 20742, USA
[4]Department of Materials Science and Engineering, The University of Tennessee, Knoxville, Tennessee 37996, USA
[5]Laboratory for Physical Sciences, College Park, Maryland 20740, USA

[a)]Author to whom correspondence should be addressed: gongc@umd.edu

ABSTRACT

Layered two-dimensional (2D) magnet/semiconductor heterostructures combine spintronic and optoelectronic properties of constituent materials, leading to new magneto-optical and magnetoelectric phenomena such as spontaneous emission of helical light and enhanced Zeeman splitting in single photon emission. While prior focus was mostly on the magnetic proximity effect, where properties of 2D magnets are transferred to nonmagnetic 2D materials, the inverse effect of 2D semiconductors altering 2D magnets is much less understood. Here, we fabricated and studied van der Waals (vdW) heterostructures of 2D magnet Fe_3GeTe_2 (FGT) and 2D semiconductor MoS_2. With reflectance magnetic circular dichroism, we found that the coercive field of MoS_2-covered FGT reduces compared with uncovered FGT, agreeing well with our first-principles calculations. With its strong spin–orbit coupling (SOC), MoS_2 effectively alters the crystal field of the adjacent FGT and its magnetic anisotropy. Furthermore, an unconventional two-step hysteresis loop emerges in MoS_2/FGT as a result of the superposition of two regions of FGT: at the interface and away from the interface. Our experimental elucidation of the SOC proximity effect that MoS_2 exerts on FGT provides fundamental understanding for the rational development of 2D magnet/semiconductor heterostructures.

Magnetic two-dimensional (2D) materials[1–5] constitute ideal platforms, where both spins and atoms are ordered in a flatland and, thus, promise a wide range of breakthroughs in scaled-down spintronics,[6] nonreciprocal flat optics,[7] tunable band topology with helicity reversal,[8] and topological magnons[9] for quantum information exchange. When 2D magnets form heterostructures with 2D semiconductors, even with short-range proximity effects, it is possible to transform their fundamental properties and realize novel functionalities.[10] For example, a WSe_2/CrI_3 heterostructure[11] can emit helical light spontaneously, and a $WSe_2/Cr_2Ge_2Te_6$ heterostructure[12] can emit single photons with strongly enhanced Zeeman splitting of excitons.

It has been well known that the interfacial phenomena can deviate from the properties of individual materials that form the interface.[10] Even across a vdW gap, electronic wavefunctions of two materials can strongly interact, as evidenced by the notable bandgap differences between monolayer (ML) and bilayer transition metal dichalcogenides (TMDs).[13,14] The dramatic roles of interlayer coupling are further demonstrated in superconducting twisted bilayer graphene,[15,16] superconducting heterostructures of trilayer graphene and boron nitride,[17,18] and Moiré excitons in TMD hetero-bilayers.[19–21] For magnetic vdW heterostructures, the existence of magnetic proximity effects with 2D materials is well established[10,11,22,23] with the typical focus on the changes in the nonmagnetic 2D materials, which acquire proximity-induced spin/valley polarization and exchange splitting. However, the inverse proximity effect of how adjacent nonmagnetic 2D materials modify 2D magnets[24] has many important ramifications[25–30] but is much less understood.

Here, we investigate the proximity effect induced by a stacked ML MoS_2 on the few-layer FGT—a prototypical itinerant 2D ferromagnet.[31] Through reflectance magnetic circular dichroism (RMCD) studies of the MoS_2/FGT heterostructure, we found that the out-of-plane coercive field (H_C) of the MoS_2-covered FGT is noticeably

reduced compared with the bare FGT. This is attributed to the enhanced in-plane magnetocrystalline anisotropy of FGT induced by the spin–orbit coupling (SOC) proximity due to the presence of MoS_2,[32] which is further corroborated by our density functional theory (DFT) calculations. Remarkably, we observed the unconventional two-step magnetic hysteresis loops that emerge at elevated temperatures (e.g., 138 K) in the MoS_2-covered FGT, which shows strong evidence that interfacial FGT layers and other FGT layers exhibit different magnetic anisotropies. Such multiple magnetization states in MoS_2/FGT heterostructures indicate device opportunities for non-von Neumann architectures and neuromorphic computing.[33,34]

In this work, few-layer FGT flakes were mechanically exfoliated onto the 260-nm-thick-SiO_2/Si substrate. The ML MoS_2 was exfoliated on polydimethylsiloxane (PDMS) and transferred onto a part of the FGT flake using the all-dry viscoelastic stamping procedure[35] [see Fig. 1(a)]. As shown in the inset of Fig. 1(a), the thickness of the FGT flake is identified by atomic force microscopy (AFM) measurements, where an 8.0 nm (estimated to be eight or nine layers (8-9L) thick, considering the possible presence of moisture or air trapped at the flake–substrate interface[36]) step can be observed in the height profile. The room-temperature Raman and photoluminescence (PL) spectra [Fig. 1(b)] taken in the MoS_2-covered region show an 18.88 cm^{-1} frequency difference between the in-plane E^1_{2g} and the out-of-plane A_{1g} modes and a strong PL emission at 672 nm, both confirming the ML thickness of MoS_2.[13,14,37] Meanwhile, no observable shift in the characteristic Raman peaks of FGT[38] (two peaks in the range of 110–160 cm^{-1}) between covered and uncovered regions suggests that there is no unintentional strain induced in the FGT flake by the stacked MoS_2 layer, making our heterostructure a clean platform for the study of the SOC proximity effect.

To probe the out-of-plane magnetic order in the MoS_2/FGT heterostructure, we employed RMCD measurements as a function of the external magnetic field applied perpendicularly to the sample plane. A 7 μW 633 nm HeNe laser with sub-micrometer spot size was focused onto the sample in the normal incidence configuration for RMCD measurements. By sweeping the magnetic field from 0.3 to −0.3 T and then from −0.3 to 0.3 T at 124 K [well below the Curie temperature of 8L FGT of 165 K (Ref. 39)], we were able to observe the near-square-shaped hysteresis loops from both the MoS_2-covered and uncovered regions. As shown in Fig. 2(a), the hysteresis loops measured at different spots in the bare FGT (represented by the red curves in the top panel) exhibit similar H_C and so do the loops measured in the covered region (represented by the blue curves in the bottom shaded panel), where the specific positions of the spots are marked in the inset of Fig. 2(b). This consistency of H_C between different spots in the same region confirms the homogeneity of our sample. More interestingly, the loops measured in the covered region are generally narrower with smaller H_C than the ones measured in the bare FGT, as shown in Fig. 2(a). Figure 2(b) displays the extracted H_C measured at different spots in both regions, showing a clear difference (∼165 Oe) in H_C of two regions on average, as indicated by the blue and red dashed lines. This reduced H_C in the MoS_2-covered FGT shows that the stacked ML MoS_2 enhances the in-plane magnetic anisotropy of the underlying FGT.

To directly visualize the different H_C of the MoS_2-covered and uncovered FGT, we conducted a RMCD mapping near the boundary of these two regions [indicated by the blue rectangle in the inset of Fig. 2(b)] at 124 K. The orientations of magnetic domains in FGT were aligned to the spin-up direction by a positive 0.3 T external magnetic field first, which is larger than the H_C of both regions. The RMCD mapping was then scanned after the magnetic field was swept from 0.3 to −0.255 T, which is strong enough to flip the magnetic domains in the MoS_2-covered FGT to spin-down but insufficient to flip the domains in bare FGT. As shown in Fig. 2(c), while the orientation of magnetization in the bare FGT remains spin-up (yellow for spin-up and blue for spin-down), the spins in the MoS_2-covered FGT are

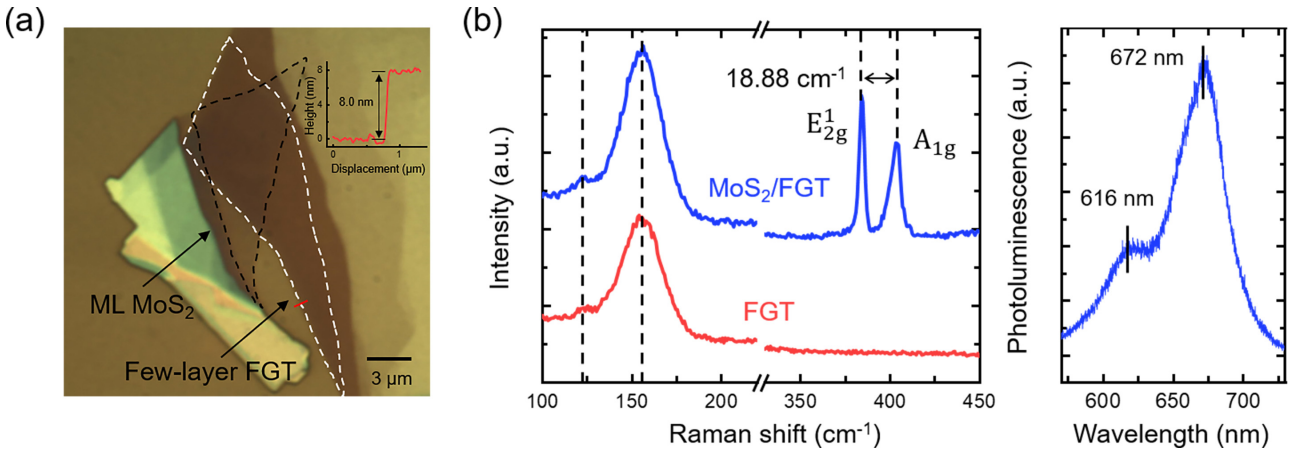

FIG. 1. AFM, Raman, and PL characterizations of the MoS_2/FGT heterostructure. (a) Optical image of the MoS_2/FGT heterostructure. The regions surrounded by the black and white dashed lines represent the top ML MoS_2 and the underneath few-layer FGT, respectively. The inset cross-sectional profile shows an 8.0 nm (8-9L, due to the presence of moisture or air trapped at the flake–substrate interface[36]) step along the red line indicated in the optical image. (b) Raman (from MoS_2-covered and uncovered regions) and PL (from the MoS_2-covered region only) spectra of the MoS_2/FGT heterostructure. The 18.88 cm^{-1} difference between two MoS_2 modes (E^1_{2g} and A_{1g}) and the strong PL emission at 672 nm in the covered region corresponds to a ML MoS_2. No noticeable shift in the FGT characteristic peaks[38] (two peaks in the range of 110–160 cm^{-1}) is observed between covered and uncovered regions, showing there is no observable strain in FGT layers unintentionally caused by MoS_2 stacking.

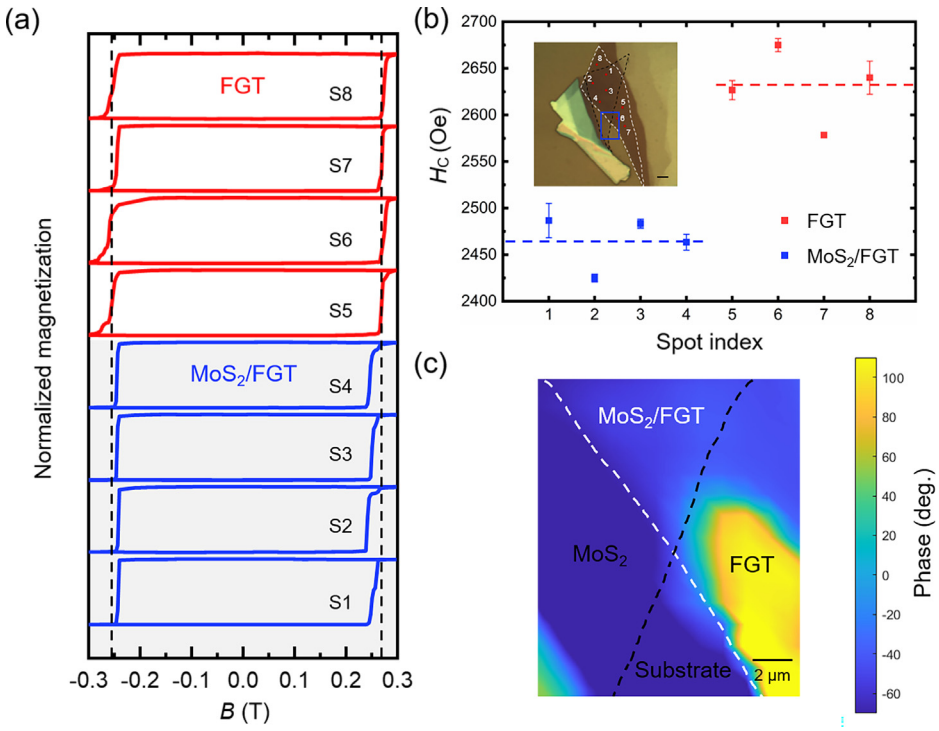

FIG. 2. RMCD measurements of the MoS_2/FGT heterostructure at 124 K. (a) Normalized magnetization measured at different spots in both MoS_2-covered and uncovered FGT. The data taken from covered and uncovered regions are represented by the blue curves in the bottom shaded panel and the red curves in the top panel, respectively. The black dashed lines serve as the eye guide by indicating the average position of coercive fields of the uncovered FGT. (b) Extracted H_C of different spots in both covered and uncovered FGT regions. The blue and red dashed lines represent the average H_C of covered and uncovered FGT, respectively. Error bars represent the standard deviations of H_C and are smaller than the plotted points if not shown. The inset is the optical image of the MoS_2/FGT heterostructure, where the specific positions of the spots are marked. Scale bar, 3 μm. (c) RMCD mapping at the boundary of covered and uncovered regions [indicated by the blue rectangle in the inset of (b)], after the external magnetic field was swept from +0.3 T (when the whole sample is magnetized to the spin-up configuration) to −0.255 T (when the bare FGT remains spin-up but the MoS_2/FGT is flipped to spin-down). The color bar is plotted by the phase of RMCD, indicating the spin-up (yellow) and spin-down (blue) domains.

flipped to the opposite direction, resulting in two opposite magnetic states alongside the stacking boundary. This serves as direct evidence that the ML MoS_2 reduces the H_C of the underlying FGT thin flake.

Owing to the extreme sensitivity of 2D layered magnets to interfacial engineering, the H_C of few-layer FGT could be affected by the stacked material via different mechanisms.[2,10] For example, since the magnetic properties critically hinge on materials' structural parameters, the magnetic anisotropy energy and exchange interaction were shown to be altered by the strain-induced lattice deformation in previous reports.[40] When the top ML MoS_2 was transferred onto the FGT flake using PDMS, unintentional strain could be introduced in FGT and, thus, affect the H_C of FGT. However, this is unlikely the scenario in our work since there is no noticeable shift in FGT's characteristic Raman peaks between MoS_2-covered and uncovered regions, as shown in Fig. 1(b). Another possible scenario is that, placing a vdW antiferromagnetic (AFM) material on top of FGT can alter its coercive field via the interfacial exchange coupling,[41,42] but this is not applicable for our experiment since MoS_2 is not magnetic on its own. Rather, our observed reduced H_C in MoS_2-covered FGT is more likely caused by the SOC proximity[26] induced by the adjacent MoS_2, which could lead to an increased in-plane magnetocrystalline anisotropy in FGT layers. Similar suppression of H_C in FGT by the current-driven modulation of SOC was also reported in the recent work.[43]

To further look into this SOC proximity effect, we performed the RMCD measurements at an elevated temperature of 138 K. Due to the stronger thermal fluctuation at elevated temperatures, the H_C of the bare FGT at 138 K decreased with respect to that at 124 K (i.e., 1850 Oe at 138 K versus 2640 Oe at 124 K), as shown by the red curve in Fig. 3(a). At 138 K, a similar reduction in the H_C of the MoS_2-covered FGT compared with that of the uncovered region is also observed. More strikingly, at 138 K, in stark contrast with the bare FGT that exhibits only two magnetic states in the hysteresis loop, the MoS_2-covered region [marked as S1–S3 in Fig. 3(a)] shows two-step loops with four stable magnetic states [highlighted by the shaded areas between dashed lines in Fig. 3(a)]. This two-step hysteresis loop can be repetitively found in different sampling spots in the MoS_2/FGT at 138 K. This clearly indicates that the FGT layers interfacing with MoS_2 and away from the interface exhibit different H_C, thereby leading to two-step hysteresis loops: while the magnetization reversal of the interfacial FGT layers occurs at a smaller external magnetic field, the underneath FGT layers require a higher magnetic field to be flipped, resulting in intermediate magnetic states between the all-spin-up and all-spin-down configurations in S1–S3 of Fig. 3(a).

These unconventional two-step hysteresis loops at the elevated temperature of 138 K indicate the difference between FGT layers at the interface and away from the interface, as illustrated in Fig. 3(b).

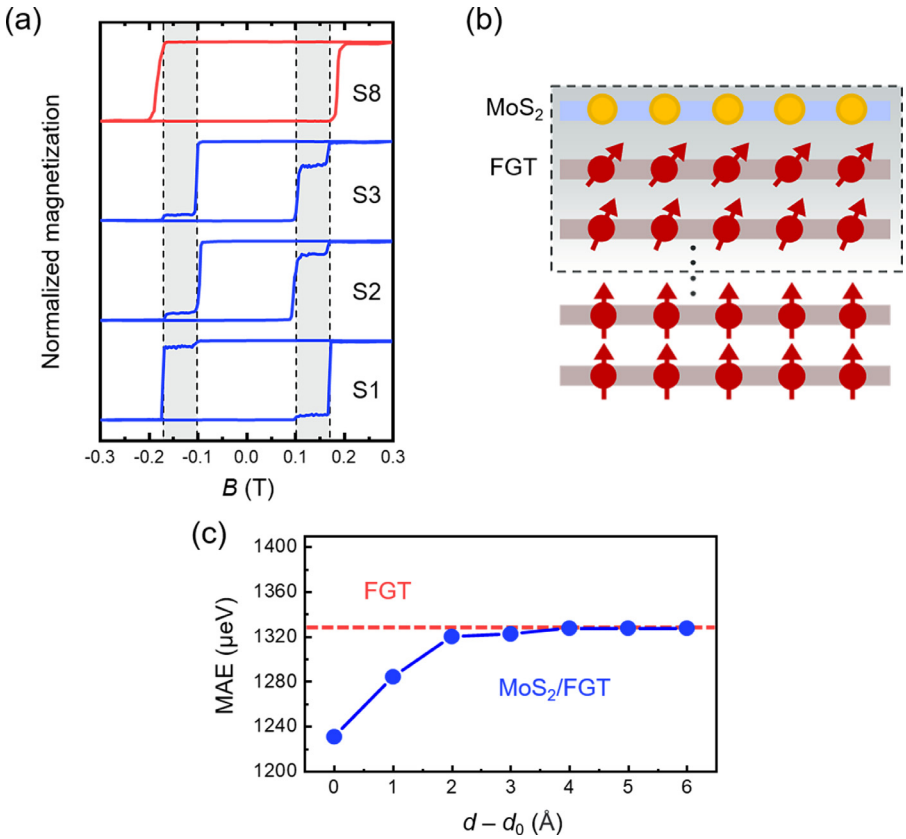

FIG. 3. RMCD measurements of the MoS_2/FGT heterostructure at 138 K and the calculated interlayer distance-dependent magnetocrystalline anisotropy energy (MAE) of MoS_2/FGT. (a) Normalized magnetization measured at different spots in MoS_2- covered and uncovered regions. The shaded areas between dashed lines highlight the intermediate magnetic states observed in the MoS_2-covered FGT. (b) Schematics of the SOC proximity effect in the MoS_2/FGT heterostructure. The solid yellow circles represent the Mo atoms in the ML MoS_2, and the solid red circles with arrows represent the magnetization orientations of different FGT layers. The shaded area inside the dashed lines depicts the interfacial FGT layers affected by the SOC proximity. (c) DFT calculation of the interlayer distance-dependent MAE in the MoS_2/FGT heterostructure. d represents the vdW distance between the ML FGT and ML MoS_2, and d_0 is the optimized distance after the structural relaxation. The red dashed line serves as an eye guide by indicating the calculated MAE of a bare ML FGT.

The SOC proximity effect originates from the interfacing with MoS_2 [Mo atoms are illustrated by the solid yellow circles in Fig. 3(b)] and the augmented SOC at the interface strongly decays into the inner layers of FGT. The short-range nature of the SOC proximity effect leads to the modified magnetocrystalline anisotropy primarily for the FGT layers at the interface, leaving the underneath FGT layers almost unaffected as shown in Fig. 3(b). At lower temperature (i.e., 124 K), the interlayer exchange coupling is less disturbed by the thermal fluctuation, and all the FGT layers behave as a whole when flipping under the external magnetic field. The observed reduced out-of-plane H_C in the MoS_2-covered FGT is an average result of the enhanced in-plane magnetic anisotropy of interfacial FGT layers and the unaffected magnetic anisotropy of the underneath FGT layers. However, as the temperature goes up, the interlayer exchange coupling becomes weaker due to the stronger thermal fluctuation and, thus, cannot maintain a uniform coercive field for the interfacial and underneath FGT layers. This explains the emergence of the two-step hysteresis loops in the MoS_2-covered region at 138 K and its apparent absence at 124 K. In addition, the interfacial Dzyaloshinskii–Moriya interaction,[44] which could possibly be induced by the strong SOC in the stacked ML MoS_2 and the broken inversion symmetry at the interface, may play a role in the canting of interfacial magnetization and, thus, altering the magnetic anisotropy of the first few FGT layers at the interface. Meanwhile, it is worth noting that the changes in the magnitude of magnetization at the intermediate step exhibit a spot dependence in the MoS_2-covered region. This is likely due to the different local contact details between the stacked MoS_2 and the underlying FGT, which again reveals the interfacial nature of the SOC proximity effect.

We performed DFT calculations to study the SOC proximity effect of MoS_2 on the magnetocrystalline anisotropy energy (MAE) of adjacent FGT, using the general potential linearized augmented plane-wave method[45] as implemented in the WIEN2k code.[46] The convergence of the calculations regarding the size of the basis set is achieved using an RMT × Kmax value of 7, where RMT (muffin-tin radius) is the smallest atomic sphere radius in the unit cell and Kmax is the magnitude of the largest K wave vector inside the first Brillouin zone (BZ). The local density approximation is used to describe the exchange and correlation functional, which can give reasonable electronic structures for FGT-based vdW heterostructures.[47,48] The Monkhorst–Pack k-grid of $18 \times 18 \times 1$ is adopted for the first BZ integral of the heterostructures. The structures were fully relaxed with an atomic force of 0.01 eV/Å, and the convergence criterion for the charge difference was <0.0001 e per unit cell. A vacuum space larger than 15 Å is set to avoid the interaction between the two adjacent heterostructure slabs. The experimental lattice constant of 3.99 Å was used for FGT calculations,[49] and 4.0% tensile strain is applied in MoS_2 to match the FGT lattice.

The MAE is defined as $E_{IP} - E_{OP}$, where E_{IP} (E_{OP}) is the total energy for the system with in-plane (out-of-plane) magnetization. For the bare ML FGT, the calculated MAE is about 1.32 meV, consistent with the previous calculations.[47] When the MoS_2/FGT (both ML) heterostructure is constructed, the MAE of FGT decreases to 1.23 meV. Such a MAE decrease confirms our experimental observation that

FGT's in-plane magnetic anisotropy is strengthened by the adjacent ML MoS_2. We further calculated the MAE of the MoS_2/FGT heterostructure as a function of their arbitrary interlayer distance d. As shown in Fig. 3(c), when $d - d_0$ ($d_0 = 3.14$ Å is the optimized distance) is relatively large, the hybridization between MoS_2 and FGT is negligible, giving rise to the same MAE as the bare ML FGT. When d decreases, their hybridization becomes stronger, resulting in the decreased MAE. Such a d-dependent MAE behavior confirms that the stacked MoS_2 can sensitively affect the magnetocrystalline anisotropy of interfacial FGT layers.

In summary, we observed the SOC proximity-induced modification of magnetic anisotropy in MoS_2/FGT heterostructures. The out-of-plane coercive field of FGT is noticeably reduced in the heterostructure, owing to the enhanced in-plane magnetocrystalline anisotropy of FGT induced by the SOC proximity of the adjacent MoS_2. The unconventional two-step hysteresis loops at elevated temperatures showcase the difference between interfacial and underneath FGT layers in the heterostructure. The multiple magnetization states in the layered magnet/semiconductor heterostructure hold technological implications in spintronics-based neuromorphic computing.[33,34] Our understanding of the SOC proximity effect in layered magnet/semiconductor heterostructures provides fundamental knowledge and valuable guidance for designing magnetic vdW heterostructures for future spintronic[50,51] and valleytronic devices.

C.G. acknowledges the support from the startup grant of the University of Maryland, College Park, and the grants from the Northrop Grumman Mission Systems' University Research Program, the Naval Air Warfare Center Aircraft Division, and the Army research laboratory cooperative via Agreement No. W911NF-19-2-0181. T.Z. and I.Ž. were supported by the U.S. DOE, Office of Science BES, Award No. DE-SC0004890 and the University at Buffalo Center for Computational Research.

AUTHOR DECLARATIONS

Conflict of Interest

The authors declare no conflict of interest.

DATA AVAILABILITY

The data that support the findings of this study are available from the corresponding author upon reasonable request.

REFERENCES

[1] C. Gong, L. Li, Z. Li, H. Ji, A. Stern, Y. Xia, T. Cao, W. Bao, C. Wang, Y. Wang, Z. Q. Qiu, R. J. Cava, S. G. Louie, J. Xia, and X. Zhang, "Discovery of intrinsic ferromagnetism in two-dimensional van der Waals crystals," Nature **546**, 265 (2017).
[2] C. Gong and X. Zhang, "Two-dimensional magnetic crystals and emergent heterostructure devices," Science **363**, eaav4450 (2019).
[3] B. Huang, G. Clark, E. Navarro-Moratalla, D. R. Klein, R. Cheng, K. L. Seyler, D. Zhong, E. Schmidgall, M. A. McGuire, D. H. Cobden, W. Yao, D. Xiao, P. Jarillo-Herrero, and X. Xu, "Layer-dependent ferromagnetism in a van der Waals crystal down to the monolayer limit," Nature **546**, 270 (2017).
[4] K. S. Burch, D. Mandrus, and J.-G. Park, "Magnetism in two-dimensional van der Waals materials," Nature **563**, 47 (2018).
[5] M. Gibertini, M. Koperski, A. F. Morpurgo, and K. S. Novoselov, "Magnetic 2D materials and heterostructures," Nat. Nanotechnol. **14**, 408 (2019).
[6] I. Žutić, J. Fabian, and S. Das Sarma, "Spintronics: Fundamentals and applications," Rev. Mod. Phys. **76**, 323 (2004).
[7] Z. Sun, Y. Yi, T. Song, G. Clark, B. Huang, Y. Shan, S. Wu, D. Huang, C. Gao, Z. Chen, M. McGuire, T. Cao, D. Xiao, W.-T. Liu, W. Yao, X. Xu, and S. Wu, "Giant nonreciprocal second-harmonic generation from antiferromagnetic bilayer CrI_3," Nature **572**, 497 (2019).
[8] G. Xu, T. Zhou, B. Scharf, and I. Žutić, "Optically probing tunable band topology in atomic monolayers," Phys. Rev. Lett. **125**, 157402 (2020).
[9] F. Zhu, L. Zhang, X. Wang, F. J. dos Santos, J. Song, T. Mueller, K. Schmalzl, W. F. Schmidt, A. Ivanov, J. T. Park, J. Xu, J. Ma, S. Lounis, S. Blügel, Y. Mokrousov, Y. Su, and T. Brückel, "Topological magnon insulators in two-dimensional van der Waals ferromagnets $CrSiTe_3$ and $CrGeTe_3$: Toward intrinsic gap-tunability," Sci. Adv. **7**, abi7532 (2021).
[10] I. Žutić, A. Matos-Abiague, B. Scharf, H. Dery, and K. Belashchenko, "Proximitized materials," Mater. Today **22**, 85 (2019).
[11] D. Zhong, K. L. Seyler, X. Linpeng, N. P. Wilson, T. Taniguchi, K. Watanabe, M. A. McGuire, K.-M. C. Fu, D. Xiao, W. Yao, and X. Xu, "Layer-resolved magnetic proximity effect in van der Waals heterostructures," Nat. Nanotechnol. **15**, 187 (2020).
[12] K. Shayan, N. Liu, A. Cupo, Y. Ma, Y. Luo, V. Meunier, and S. Strauf, "Magnetic proximity coupling of quantum emitters in WSe_2 to van der Waals ferromagnets," Nano Lett. **19**, 7301 (2019).
[13] A. Splendiani, L. Sun, Y. Zhang, T. Li, J. Kim, C.-Y. Chim, G. Galli, and F. Wang, "Emerging photoluminescence in monolayer MoS_2," Nano Lett. **10**, 1271 (2010).
[14] K. F. Mak, C. Lee, J. Hone, J. Shan, and T. F. Heinz, "Atomically thin MoS_2: A new direct-gap semiconductor," Phys. Rev. Lett. **105**, 136805 (2010).
[15] Y. Cao, V. Fatemi, S. Fang, K. Watanabe, T. Taniguchi, E. Kaxiras, and P. Jarillo-Herrero, "Unconventional superconductivity in magic-angle graphene superlattices," Nature **556**, 43 (2018).
[16] Y. Cao, V. Fatemi, A. Demir, S. Fang, S. L. Tomarken, J. Y. Luo, J. D. Sanchez-Yamagishi, K. Watanabe, T. Taniguchi, E. Kaxiras, R. C. Ashoori, and P. Jarillo-Herrero, "Correlated insulator behaviour at half-filling in magic-angle graphene superlattices," Nature **556**, 80 (2018).
[17] G. Chen, L. Jiang, S. Wu, B. Lyu, H. Li, B. L. Chittari, K. Watanabe, T. Taniguchi, Z. Shi, J. Jung, Y. Zhang, and F. Wang, "Evidence of a gate-tunable Mott insulator in a trilayer graphene moiré superlattice," Nat. Phys. **15**, 237 (2019).
[18] G. Chen, A. L. Sharpe, P. Gallagher, I. T. Rosen, E. J. Fox, L. Jiang, B. Lyu, H. Li, K. Watanabe, T. Taniguchi, J. Jung, Z. Shi, D. Goldhaber-Gordon, Y. Zhang, and F. Wang, "Signatures of tunable superconductivity in a trilayer graphene moiré superlattice," Nature **572**, 215 (2019).
[19] K. L. Seyler, P. Rivera, H. Yu, N. P. Wilson, E. L. Ray, D. G. Mandrus, J. Yan, W. Yao, and X. Xu, "Signatures of moiré-trapped valley excitons in $MoSe_2$/WSe_2 heterobilayers," Nature **567**, 66 (2019).
[20] K. Tran, G. Moody, F. Wu, X. Lu, J. Choi, K. Kim, A. Rai, D. A. Sanchez, J. Quan, A. Singh, J. Embley, A. Zepeda, M. Campbell, T. Autry, T. Taniguchi, K. Watanabe, N. Lu, S. K. Banerjee, K. L. Silverman, S. Kim, E. Tutuc, L. Yang, A. H. MacDonald, and X. Li, "Evidence for moiré excitons in van der Waals heterostructures," Nature **567**, 71 (2019).
[21] C. Jin, E. C. Regan, A. Yan, M. I. B. Utama, D. Wang, S. Zhao, Y. Qin, S. Yang, Z. Zheng, S. Shi, K. Watanabe, T. Taniguchi, S. Tongay, A. Zettl, and F. Wang, "Observation of moiré excitons in WSe_2/WS_2 heterostructure superlattices," Nature **567**, 76 (2019).
[22] C. Zhao, T. Norden, P. Zhang, P. Zhao, Y. Cheng, F. Sun, J. P. Parry, P. Taheri, J. Wang, Y. Yang, T. Scrace, K. Kang, S. Yang, G. Miao, R. Sabirianov, G. Kioseoglou, W. Huang, A. Petrou, and H. Zeng, "Enhanced valley splitting in monolayer WSe_2 due to magnetic exchange field," Nat. Nanotechnol. **12**, 757 (2017).
[23] J. Xu, S. Singh, J. Katoch, G. Wu, T. Zhu, I. Žutić, and R. K. Kawakami, "Spin inversion in graphene spin valves by gate-tunable magnetic proximity effect at one-dimensional contacts," Nat. Commun. **9**, 2869 (2018).
[24] C. Gong, E. M. Kim, Y. Wang, G. Lee, and X. Zhang, "Multiferroicity in atomic van der Waals heterostructures," Nat. Commun. **10**, 2657 (2019).
[25] M. H. D. Guimarães, G. M. Stiehl, D. MacNeill, N. D. Reynolds, and D. C. Ralph, "Spin-orbit torques in $NbSe_2$/permalloy bilayers," Nano Lett. **18**, 1311 (2018).
[26] J. F. Sierra, J. Fabian, R. K. Kawakami, S. Roche, and S. O. Valenzuela, "Van der Waals heterostructures for spintronics and opto-spintronics," Nat. Nanotechnol. **16**, 856 (2021).
[27] K. Dolui, M. D. Petrović, K. Zollner, P. Plecháč, J. Fabian, and B. K. Nikolić, "Proximity spin-orbit torque on a two-dimensional magnet within van der Waals

heterostructure: Current-driven antiferromagnet-to-ferromagnet reversible non-equilibrium phase transition in bilayer CrI_3," Nano Lett. **20**, 2288 (2020).
[28]K. Zollner, M. D. Petrović, K. Dolui, P. Plecháč, B. K. Nikolić, and J. Fabian, "Scattering-induced and highly tunable by gate damping-like spin-orbit torque in graphene doubly proximitized by two-dimensional magnet $Cr_2Ge_2Te_6$ and monolayer WS_2," Phys. Rev. Res. **2**, 043057 (2020).
[29]S. J. Gong, Z. Y. Li, Z. Q. Yang, C. Gong, C.-G. Duan, and J. H. Chu, "Spintronic properties of graphene films grown on Ni(111) substrate," J. Appl. Phys. **110**, 043704 (2011).
[30]H. Yang, G. Chen, A. A. C. Cotta, A. T. N'Diaye, S. A. Nikolaev, E. A. Soares, W. A. A. Macedo, K. Liu, A. K. Schmid, A. Fert, and M. Chshiev, "Significant Dzyaloshinskii-Moriya interaction at graphene-ferromagnet interfaces due to the Rashba effect," Nat. Mater. **17**, 605 (2018).
[31]Y. Deng, Y. Yu, Y. Song, J. Zhang, N. Z. Wang, Z. Sun, Y. Yi, Y. Z. Wu, S. Wu, J. Zhu, J. Wang, X. H. Chen, and Y. Zhang, "Gate-tunable room-temperature ferromagnetism in two-dimensional Fe_3GeTe_2," Nature **563**, 94 (2018).
[32]Z. Y. Zhu, Y. C. Cheng, and U. Schwingenschlögl, "Giant spin-orbit-induced spin splitting in two-dimensional transition-metal dichalcogenide semiconductors," Phys. Rev. B **84**, 153402 (2011).
[33]J. Grollier, D. Querlioz, K. Y. Camsari, K. Everschor-Sitte, S. Fukami, and M. D. Stiles, "Neuromorphic spintronics," Nat. Electron. **3**, 360 (2020).
[34]C. Cui, O. G. Akinola, N. Hassan, C. H. Bennett, M. J. Marinella, J. S. Friedman, and J. A. C. Incorvia, "Maximized lateral inhibition in paired magnetic domain wall racetracks for neuromorphic computing," Nanotechnology **31**, 294001 (2020).
[35]A. Castellanos-Gomez, M. Buscema, R. Molenaar, V. Singh, L. Janssen, H. S. J. van der Zant, and G. A. Steele, "Deterministic transfer of two-dimensional materials by all-dry viscoelastic stamping," 2D Mater. **1**, 011002 (2014).
[36]P. Nemes-Incze, Z. Osváth, K. Kamarás, and L. P. Biró, "Anomalies in thickness measurements of graphene and few layer graphite crystals by tapping mode atomic force microscopy," Carbon **46**, 1435 (2008).
[37]C. Lee, H. Yan, L. E. Brus, T. F. Heinz, J. Hone, and S. Ryu, "Anomalous lattice vibrations of single- and few-layer MoS_2," ACS Nano **4**, 2695 (2010).
[38]L. Du, J. Tang, Y. Zhao, X. Li, R. Yang, X. Hu, X. Bai, X. Wang, K. Watanabe, T. Taniguchi, D. Shi, G. Yu, X. Bai, T. Hasan, G. Zhang, and Z. Sun, "Lattice dynamics, phonon chirality, and spin-phonon coupling in 2D itinerant ferromagnet Fe_3GeTe_2," Adv. Funct. Mater. **29**, 1904734 (2019).
[39]Z. Tu, T. Xie, Y. Lee, J. Zhou, A. S. Admasu, Y. Gong, N. Valanoor, J. Cumings, S.-W. Cheong, I. Takeuchi, K. Cho, and C. Gong, "Ambient effect on the Curie temperatures and magnetic domains in metallic two-dimensional magnets," npj 2D Mater. Appl. **5**, 62 (2021).
[40]Y. Wang, C. Wang, S. Liang, Z. Ma, K. Xu, X. Liu, L. Zhang, A. S. Admasu, S.-W. Cheong, L. Wang, M. Chen, Z. Liu, B. Cheng, W. Ji, and F. Miao, "Strain-sensitive magnetization reversal of a van der Waals magnet," Adv. Mater. **32**, 2004533 (2020).
[41]R. Zhu, W. Zhang, W. Shen, P. K. J. Wong, Q. Wang, Q. Liang, Z. Tian, Y. Zhai, C. Qiu, and A. T. S. Wee, "Exchange bias in van der Waals $CrCl_3$/Fe_3GeTe_2 Heterostructures," Nano Lett. **20**, 5030 (2020).
[42]L. Zhang, X. Huang, H. Dai, M. Wang, H. Cheng, L. Tong, Z. Li, X. Han, X. Wang, L. Ye, and J. Han, "Proximity-coupling-induced significant enhancement of coercive field and Curie temperature in 2D van der Waals heterostructures," Adv. Mater. **32**, 2002032 (2020).
[43]K. Zhang, S. Han, Y. Lee, M. J. Coak, J. Kim, I. Hwang, S. Son, J. Shin, M. Lim, D. Jo, K. Kim, D. Kim, H. W. Lee, and J. G. Park, "Gigantic current control of coercive field and magnetic memory based on nanometer-thin ferromagnetic van der Waals Fe_3GeTe_2," Adv. Mater. **33**, 2004110 (2021).
[44]A. Kumar, A. K. Chaurasiya, N. Chowdhury, A. K. Mondal, R. Bansal, A. Barvat, S. P. Khanna, P. Pal, S. Chaudhary, A. Barman, and P. K. Muduli, "Direct measurement of interfacial Dzyaloshinskii–Moriya interaction at the MoS_2/$Ni_{80}Fe_{20}$ interface," Appl. Phys. Lett. **116**, 232405 (2020).
[45]D. J. Singh and L. Nordstrom, *Planewaves, Pseudopotentials and the LAPW Method*, 2nd ed. (Springer, New York, 2006).
[46]P. Blaha, K. Schwarz, G. K. H. Madsen, D. Kvasnicka, and J. Luitz, *An Augmented Plane Wave + Local Orbitals Program for Calculating Crystal Properties* (Technische Universitat Wien, Vienna, 2001).
[47]H. L. Zhuang, P. R. C. Kent, and R. G. Hennig, "Strong anisotropy and magnetostriction in the two-dimensional Stoner ferromagnet Fe_3GeTe_2," Phys. Rev. B **93**, 134407 (2016).
[48]W. Zhu, H. Lin, F. Yan, C. Hu, Z. Wang, L. Zhao, Y. Deng, Z. R. Kudrynskyi, T. Zhou, Z. D. Kovalyuk, Y. Zheng, A. Patanè, I. Žutić, S. Li, H. Zheng, and K. Wang, "Large tunneling magnetoresistance in van der Waals ferromagnet/semiconductor heterojunctions," Adv. Mater. **33**, 2104658 (2021).
[49]H.-J. Deiseroth, K. Aleksandrov, C. Reiner, L. Kienle, and R. K. Kremer, "Fe_3GeTe_2 and Ni_3GeTe_2 – two new layered transition-metal compounds: Crystal structures, HRTEM investigations, and magnetic and electrical properties," Eur. J. Inorg. Chem. **2006**, 1561.
[50]S.-J. Gong, C. Gong, Y. Sun, W. Tong, C. Duan, J. Chu, and X. Zhang, "Electrically induced 2D half-metallic antiferromagnets and spin field effect transistors," Proc. Natl. Acad. Sci. **115**, 8511–8516 (2018).
[51]E.-W. Du, S.-J. Gong, X. Tang, J. Chu, A. M. Rappe, and C. Gong, "Ferroelectric switching of pure spin polarization in two-dimensional electron gas," Nano Lett. **20**, 7230–7236 (2020).